Astron. Astrophys. 333, 813–826 (1998)

ASTRONOMY AND ASTROPHYSICS

# Young tidal dwarf galaxies around the gas-rich disturbed lenticular NGC 5291⋆

**P.-A. Duc**[1] **and I.F. Mirabel**[2]

[1] ESO, Karl-Schwarzschild-Strasse 2, D-85748 Garching bei München, Germany
[2] CEA, SAp, C.E. Saclay, F-91191 Gif-sur-Yvette Cedex, France & Instituto de Astronomía y Física del Espacio, Argentina

Received 25 September 1997 / Accepted 9 December 1997

**Abstract.** NGC 5291 is an early type galaxy at the edge of the cluster Abell 3574 which drew the attention because of the unusual high amount of atomic gas ($\sim 5\times10^{10}$ $M_\odot$) found associated to it. The HI is distributed along a huge and fragmented ring, possibly formed after a tidal interaction with a companion galaxy. We present multi-slit optical spectroscopic observations and optical/near-infrared images of the system. We show that NGC 5291 is a LINER galaxy exhibiting several remnants of previous merging events, in particular a curved dust lane and a counter-rotation of the gas with respect to the stars. The atomic hydrogen has undoubtly an external origin and was probably accreted by the galaxy from a gas-rich object in the cluster. It is unlikely that the HI comes from the closest companion of NGC 5291, the so-called "Seashell" galaxy, which appears to be a fly-by object at a velocity greater than 400 km $s^{-1}$.

We have analyzed the properties of 11 optical counterparts to the clumps observed in the HI ring. The brightest knots show strong similarities with classical blue compact dwarf galaxies. They are dominated by active star forming regions; their most recent starburst is younger than 5 Myr; we did not find evidences for the presence of an old underlying stellar population. NGC 5291 appears to be a maternity of extremely young objects most probably forming their first generation of stars. Born in pre-enriched gas clouds, these recycled galaxies have an oxygen abundance which is higher than BCDGs ($Z_\odot/3$ on average) and which departs from the luminosity–metallicity relation observed for typical dwarf and giant galaxies. We propose this property as a tool to identify tidal dwarf galaxies (TDGs) among the dwarf galaxy population. Several TDGs in NGC 5291 exhibit strong velocity gradients in their ionized gas and may already be dynamically independent galaxies.

**Key words:** galaxies: individual: NGC 5291 – galaxies: interactions – galaxies: formation – galaxies: ISM – galaxies: dwarf – radio lines: galaxies

## 1. Introduction

The formation of galaxies is still largely poorly understood. Young galaxies producing their first generation of stars are hence actively searched. The favorite and natural target is the distant – early – Universe; in the nearby Universe, metal deficient blue compact dwarf galaxies (hereafter BCDGs) embedded in large presumably primordial HI clouds are also good candidates (e.g. Thuan et al. 1997) although most of them may have an underlying old stellar component (Papaderos et al. 1996; Doublier & Caulet 1996). Another class of young galaxies has emerged from recent studies of interacting galaxies: the so-called "tidal dwarf galaxies" (hereafter TDGs), formed out of gaseous and stellar material tidally pulled out in the intergalactic medium from interacting parent galaxies (Schweizer 1978; Hibbard et al. 1994; Duc 1995; Duc & Mirabel 1997; see also review by Sanders & Mirabel 1996). These recycled objects are interesting to study in the framework of galaxy formation because, contrary to the BCDGs, an upper limit can be given for their age: the epoch of the collision between their parent galaxies that can be estimated thanks to numerical simulations. Most often star-forming TDGs are found at the end of the long stellar tails observed in interacting systems. Of special interest though are objects born in HI tidal tails not contaminated by an old stellar component expelled from the parent disks. This occurs in systems involving early-type galaxies for which stellar tails are difficult to produce.

A remarkable example of such objects is NGC 5291. It is composed of a perturbed elliptical or lenticular galaxy, NGC 5291, in close interaction with a disturbed galaxy, known at the "Seashell" because of its suggestive morphology. Both galaxies have a projected separation of 12 kpc. They belong to the outer region of a cluster of galaxies, Abell 3574 (also known as IC 4329 and Klemola 27) and are situated at a distance of 58 Mpc [1]. Longmore et al. (1979) (hereafter L79) noticed on a Schmidt plate the presence of faint knotty extensions distributed along an arc crossing NGC 5291. But contrary to what is observed in classical disk-disk systems, these knots do not form

*Send offprint requests to*: pduc@eso.org

⋆ Based on observations collected at the European Southern Observatory, La Silla, Chile. ESO N$^o$ 53.1-076 and ESO N$^o$ 56.A-0757

[1] In this paper we use $H_0 = 75$ km $s^{-1}$ $Mpc^{-1}$. At the distance of NGC 5291, 1" = 0.28 kpc.

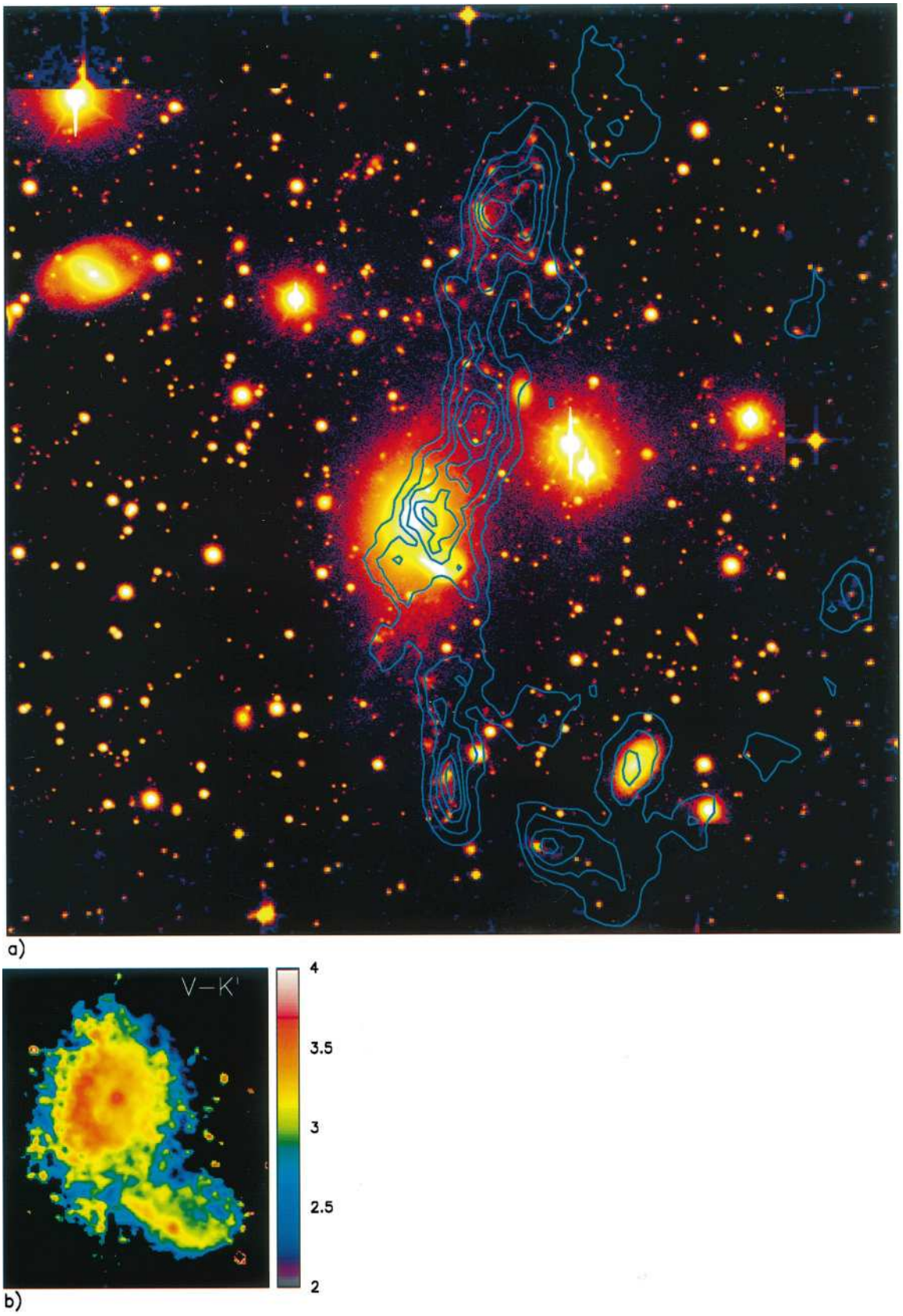


**Fig. 1.** **a** Optical R band NTT image of the colliding system NGC 5291 in the cluster Abell 3574. The main protagonists are a lenticular galaxy, NGC 5291, and a disturbed galaxy, "the Seashell", a fly-by object at velocity greater than 400 km $s^{-1}$. The VLA HI contours from Malphrus et al. (1997) are superimposed in blue on the main image. A wider-field image from the Digitized Sky Survey has been inserted under the CCD frame to cover all the gas extension. Most HI peaks have optical counterparts identified as giant HII regions, with properties similar to star-forming dwarf galaxies. The total field of view is $10'.5 \times 10'.9$ ($176 \times 183$ kpc). North is up and East to the left. **b** V-K' color map of NGC 5291/Seashell. Obscured regions, such as dust lanes, show up in red. Foreground stars have been subtracted.

**Table 1.** Observational parameters

| | |
|---|---|
| Optical imaging | ESO 3.5m + EMMI (red branch) |
| | Date: July 1994 |
| | CCD: Tektronix $2048^2$, 027"/px |
| | Filters: Bb,V,R |
| | Exposure time: 5 min |
| Spectroscopy | EMMI - Multi-Object Spectroscopy |
| | Date: July 1994 |
| | Slit width: 1.5" |
| | Grism: ESO#3, 2.26 Å/px |
| | Exposure time: $4 \times 30$ min |
| NIR imaging | ESO/MPI 2.2m + IRAC2B |
| | Date: February 1996 |
| | Detector: NICMOS 3, $256^2$, 0.49"/px |
| | Filters: J,H,K' |
| | Exposure time: $32 \times 1$ min |
| | (mosaic) |

a continuous optical tail. L79 took the spectra of the brightest knots and identified them as giant extragalactic HII regions. Single dish 21 cm observations revealed the presence in that system of unusual quantities of atomic hydrogen (L79). Recently Malphrus et al. (1997) (hereafter MSGH97) published a map of the HI gas observed with the Very Large Array. They showed that the atomic hydrogen forms a huge asymmetric and clumpy ring with a diameter of $\sim 200$ kpc. The HI clumps appear to be associated with the optical knots discovered by L79. Incidentally some spectrophotometric information is available in the literature for one of the knots that showed up in an Object Prism Survey of HII galaxies (Maza et al. 1991; Peña et al. 1991).

We report here a detailed optical and near-infrared study of NGC 5291, focussed on its extragalactic HII regions. Using multi-object spectroscopy and BVRJHK' imaging, we have analyzed the properties of these objects. We present in Sect. 2 the observations and data-reduction; we describe in Sect. 3 the protagonists of the interaction, and finally discuss in Sect. 4 the physics and origin of the forming galaxies.

## 2. Observations and data-reduction

All observations of NGC 5291 have been carried out at la Silla (ESO). Observing parameters are summarized in Table 1.

### *2.1. Optical and near-infrared imaging*

Large field optical B,V,R images were obtained in July 1994 using EMMI installed on the 3.5m NTT telescope under poor seeing conditions (2"). An R image of the field is shown in Fig. 1. Several photometric standard fields (Landolt 1992) were observed during the run.

Near-infrared J,H and K' images of the system were obtained in February 1996 at the ESO/MPI 2.2m telescope with the IRAC 2B instrument. Because of the small field of view of the camera (2' in the configuration we used) compared to the total size of the system ($\sim$10'), we had to mosaic the field. Images

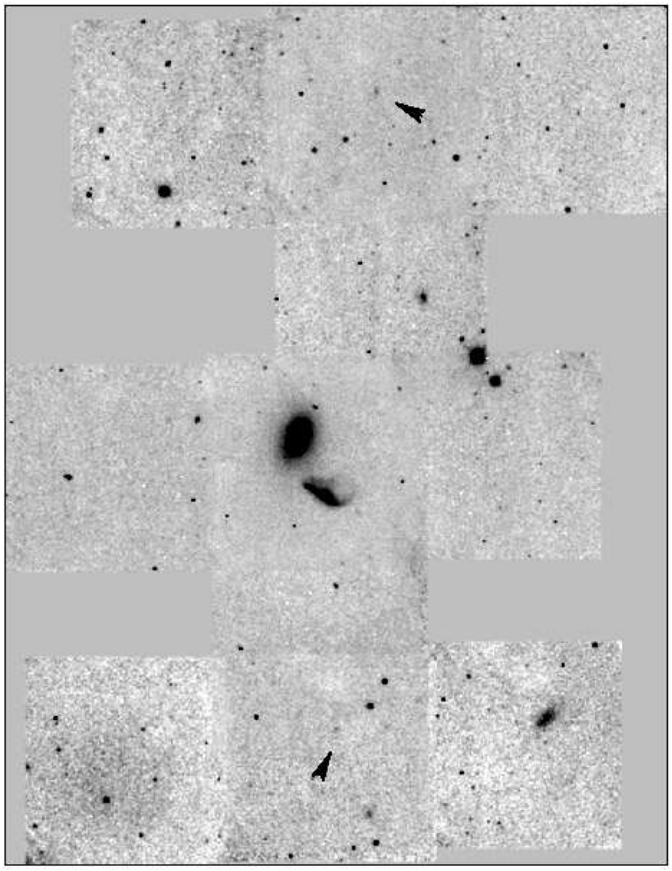

**Fig. 2.** Near-infrared recombined K' image of the field around NGC 5291, obtained with IRAC2 at the ESO/MPI 2.2m telescope. The two brightest tidal dwarfs are detected and indicated by the arrows. The flanking noisy frames have lower integration time.

were centered on three areas: on NGC 5291 itself, on region situated 3' to the South, and on a region situated 4' to the North. Sky images were obtained from adjacent fields offseted by 2'. That way, the entire system was covered although the actual total integration time was higher on the three principal fields. Several photometric standard stars from the list of UKIRT faint IR standards (Casali & Hawarden 1992) were observed under photometric conditions.

The data reduction of the optical images involved classical procedures carried out with the CCDRED package within IRAF. The data reduction of the infrared images were carried out with scripts using IRAF build-in procedures. The images were dark subtracted and flat-fielded with dome flats. Illumination corrections were done using an illumination frame created from a star scan on 18 positions on the detector. All images have then been sky-subtracted with sky images obtained by median filtering the jittered adjacent frames. They were then registered to a reference optical CCD image. The final combination was performed by the "imcombine" IRAF procedure, after rejecting some files showing inhomogeneous background. Fig. 2 displays the recombined K' image of the field.

Aperture photometry was carried out in all optical and broad-band filters, using the same aperture. The frames had pre-

**Table 2.** Properties of the parent galaxies

| | NGC 5291 | Seashell |
|---|---|---|
| Adopted distance [a] | 58 Mpc | 58 Mpc |
| Optical velocity | 4350 km s$^{-1}$ | 3941 km s$^{-1}$ [b] |
| Galactic extinction | 0.19 mag | 0.19 mag |
| $M_B$ | -20.3 | -19.1 |
| B | 13.73 | 14.94 |
| V | 12.68 | 13.93 |
| R | 12.14 | 13.44 |
| J | 10.41 | 11.72 |
| H | 9.72 | 11.02 |
| K' | 9.36 | 10.63 |
| | HII region in NGC 5291 | |
| $A_B$ | 1.7 mag | |
| $H_\beta$ flux | $6.31\times10^{-16}$ erg cm$^{-2}$ s$^{-1}$ | |
| $I$(OIII4959+5007)/$I(H_\beta)$ | 1.0 | |
| 12+log(O/H) | 8.7 | |

[a]: $H_0 = 75$ km s$^{-1}$ Mpc$^{-1}$
[b]: L79 found 3730 km s$^{-1}$

viously been registered and PSF-matched. This was important since the images were obtained in various seeing conditions, from 1" in the NIR to 2" in the R band. Table 2 and Table 4 display the magnitudes of resp. the parent galaxies and the optical knots identified in Table 3 and Fig. 3a–d. The optical photometry obtained for NGC 5291 and the Seashell is in good agreement – within 0.1 mag – with photometric data from the literature (Daly et al. 1987; Smith & Hintzen 1991). The magnitudes presented in Table 2 were obtained with a fixed polygonal aperture whereas the magnitudes in Table 4 were measured within a circular aperture with a radius given in Col. 3. Associated accuracies are given in Table 4.

### *2.2. Optical spectroscopy*

We have used the multi-slit spectroscopic capabilities of EMMI to simultaneously take spectra of several dwarf galaxy candidates. 17 fuzzy galaxy-like objects have been selected from the optical image on the southern and northern sides of NGC 5291 in regions where L79 had detected HI emission. Their positions are indicated in Fig. 3a–d. The slit lengths were adjusted to include enough sky emission. Three longer slits were punched along a South–North axis encompassing the nuclei of NGC 5291, the Seashell and a small galaxy to the North–West of NGC 5291, labeled as "C" on Fig.3a–d. Three stars in the field were also chosen for accurate positioning of the mask. Four exposures of 30 minutes each were obtained with a low resolution grism covering the 4500-7800 Å wavelength range. Several spectrophotometric standards from the list of Hamuy et al. (1992) were observed during the run.

MOS files were bias subtracted and flat-fielded using a spectroscopic flat obtained with an internal lamp. Wavelength calibration was performed from He Ar lamp observations. A second order wavelength calibration was done with the O sky emission lines. The velocity accuracy reached is better than 30 km s$^{-1}$. The extraction of the individual spectra was not straightforward because of the severe distortions in the MOS frame. Most objects exhibit strong emission lines and a very weak continuum. Therefore a direct tracing of the spectra along the wavelength axis was not possible. Instead, we have traced the sky continuum emission along the slit edge, applied the derived polynomial fit to the object spectra and checked that the extraction apertures were centered on all emission line peaks. A 10 % accuracy for the absolute flux calibration was obtained from the spectroscopic standards. A sky extinction curve typical for la Silla Observatory was applied to the spectra. Potential illumination problems in the MOS field were investigated from the spatial distribution of O sky lines in the MOS frames. The flux variations are less than 10 %. Line fluxes and errors were measured with gaussian fittings with the IRAF "splot" procedure. The [NII]$\lambda6548, 6584$, $H_\alpha$ and [SII]$\lambda6717, 6731$ lines were deblended. Data were corrected for extinction using the formula:

$$\frac{I(\lambda)}{I(H_\beta)} = \frac{F(\lambda)}{F(H_\beta)} * 10^{c*f(\lambda)}$$

where $F(\lambda)$ is the observed line flux, $f(\lambda)$, the redenning function taken from Torres-Peimbert et al. (1989) and $c$ the logarithm reddening correction at $H_\beta$ obtained from a theoretical $H_\alpha/H_\beta$ Balmer decrement of 2.85. The lines were not corrected for underlying stellar absorption. Tables 5,6 display the values of $f$, $c$, the absolute flux and equivalent width of the $H_\beta$ line and the observed/corrected fluxes relative to $H_\beta$ of the principal lines. For objects with detected $H_\alpha$, $H_\beta$ and $H_\gamma$ Balmer lines, we checked whether the Balmer line decrements $H_\alpha/H_\beta$ and $H_\beta/H_\gamma$ were consistent with each other. This allowed us to ensure a level of confidence of 5 % for the relative spectrophotometry for the brightest lines of objects with $H_\beta$ fluxes greater than $5\times10^{-16}$ erg cm$^{-2}$ s$^{-1}$. Those are listed in Table 5 whereas the objects with less good spectrophotometry are listed in Table 6. Dubious values are marked with ":". "-" indicates lines that have not been detected and "+" lines that could not be measured because they were outside our spectral range.

We compared our spectrophotometry to the limited data set presented in L79. We found at most 20 % differences for the main line fluxes of Knot a and i (F and B in L79). Peña et al. (1991) took also a spectrum of Knot i (K09.09 in this reference). The agreement with our measurements is better than 10 % for the absolute spectrophotometry and 3 % for the line ratios.

## 3. Results

Fig. 1 displays an optical CCD image of the region around NGC 5291, with superimposed on it, HI contours from MSGH97. We describe hereafter the principal protagonists involved in the collision witnessed in the figure: NGC 5291, the Seashell, and the optical counterparts of the huge HI ring.

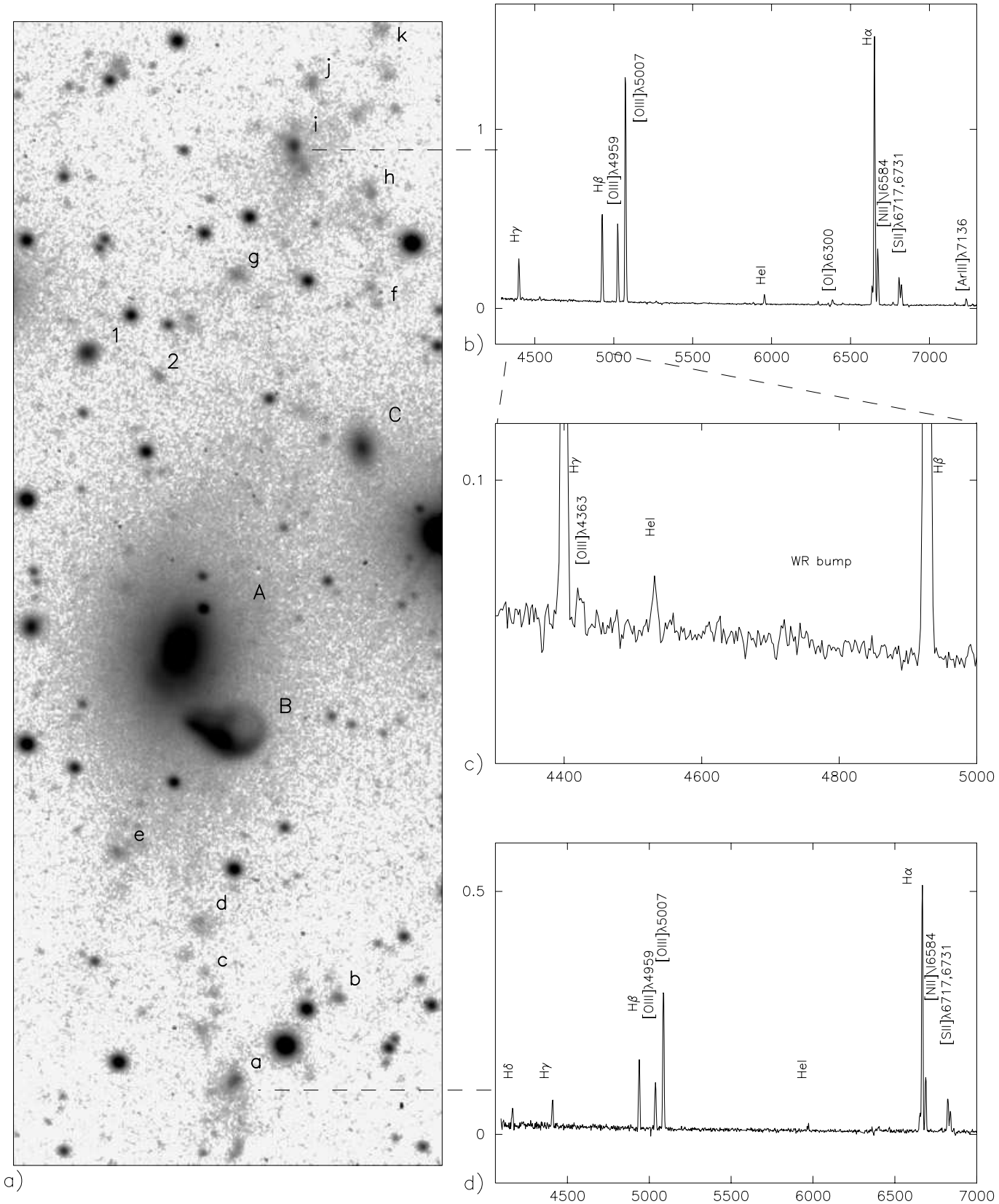


**Fig. 3a–d.** MOS observations of the region around NGC 5291. **a** Identification chart: the objects for which spectra were obtained are labeled with upper case letters for the cluster galaxies, lower case letters for the optical knots and numbers for identified background galaxies. **b–d** Optical spectra of the two brightest optical knots in the HI ring (Knot a,i). Flux units are $10^{-15}$ erg cm$^{-2}$ s$^{-1}$ Å$^{-1}$.

**Table 3.** Identification of the optical knots (km $s^{-1}$)

| Object | L79 Name | RA J2000 | DEC J2000 | $V_{opt}$ km $s^{-1}$ | L79 $V_{opt}$ km $s^{-1}$ | $V_{HI}$ km $s^{-1}$ |
|---|---|---|---|---|---|---|
| (1) | (2) | (3) | (4) | (5) | (6) | (7) |
| Knot a | Knot F | 13:47:23.0 | -30:27:30 | 4642 ± 5 | 4645 | 4645 |
| Knot b | Knot M | 13:47:19.5 | -30:26:55 | 4536 ± 12 | | 4645 |
| Knot c | | 13:47:23.8 | -30:26:43 | 4617 ± 14 | | 4666 |
| Knot d | Knot D | 13:47:24.0 | -30:26:21 | 4571 ± 29 | 4630 | 4577 |
| Knot e | Knot C | 13:47:26.6 | -30:25:51 | 4415 ± 3 | 4515 | 4666 |
| Knot f | | 13:47:17.9 | -30:21:58 | 4035 ± 35 | | 4121 |
| Knot g | | 13:47:22.5 | -30:21:46 | 4162 ± 2 | | 4192 |
| Knot h | | 13:47:18.0 | -30:21:11 | 4098 ± 2 | | 4138 |
| Knot i | Knot B | 13:47:20.5 | -30:20:51 | 3996 ± 11 | 4110 | 4143 |
| Knot j | Knot A | 13:47:20.0 | -30:20:25 | 4075 ± 6 | 4100 | 4131 |
| Knot k | | 13:47:17.6 | -30:20:02 | 4041 ± 13 | | 4105 |

**Table 4.** Photometry of the optical knots

| Name | aperture arcsec | B mag | V mag | R mag | J mag | H mag | K' mag |
|---|---|---|---|---|---|---|---|
| Knot a | 4.0 | 18.87±0.01 | 18.63±0.01 | 18.29±0.01 | 17.90±0.05 | 17.68±0.15 | 16.50±0.07 |
| | 10.5 | 18.46±0.01 | 18.20±0.01 | 17.88±0.01 | | | |
| Knot b | 5.5 | 19.87±0.02 | 19.61±0.03 | 19.35±0.02 | | | |
| Knot c | 2.5 | 21.88±0.08 | 21.65±0.10 | 21.22±0.05 | | | |
| Knot d | 6.5 | 20.17±0.05 | 19.69±0.04 | 19.30±0.03 | | | |
| Knot e | 9.5 | 19.43±0.03 | 18.91±0.03 | 18.48±0.01 | | | |
| Knot f | 3.5 | 21.32±0.10 | 21.00±0.10 | 20.57±0.04 | | | |
| Knot g | 6.0 | 19.85±0.03 | 19.39±0.03 | 19.03±0.02 | | | |
| Knot h | 5.0 | 20.03±0.03 | 19.76±0.03 | 19.33±0.02 | | | |
| Knot i | 5.0 | 18.27±0.01 | 17.91±0.01 | 17.61±0.01 | 16.94±0.04 | 16.53±0.04 | 15.79±0.04 |
| | 13.5 | 17.62±0.01 | 17.27±0.01 | 16.97±0.01 | | | |
| Knot j | 4.0 | 20.27±0.03 | 20.01±0.03 | 19.61±0.02 | | | |
| Knot k | 4.5 | 20.61±0.04 | 20.21±0.04 | 19.73±0.02 | | | |

### *3.1. NGC 5291*

NGC 5291 is classified as a peculiar elliptical (RC3, Daly et al. 1987) although its disturbed morphology and color suggest more the presence of an S0 disk. Distortions of the elliptical isophotes are clearly visible in the outer South-East region (see Fig. 4a). The V-K' color map, shown in Fig. 1b, reveals the presence of a dust lane, forming to the East an arc along the major axis at a nuclear distance of 10" (2.8 kpc). The V-K' color index in and outside the dust lane differs by 0.3 mag. If this difference is due to extinction, the dust lane has at least 0.4 mag of blue absorption. The galaxy was however not detected in the far-infrared during the IRAS mission.

The spectrum of its nucleus (see Fig. 4d) exhibits Balmer and forbidden [OIII],[NII] and [SII] lines in emission buried in an elliptical-like spectrum. Stellar features were subtracted from the spectrum using the E2 galaxy NGC 4478 as a template. Routines developed by E. Emsellem under MIDAS (Emsellem et al. 1997, in preparation) were used to that purpose. The line ratios of the emission lines measured on the stellar-free spectrum ($[NII]_{\lambda 6584}/H_{\alpha} = 1.0$ and $[OIII]_{\lambda 5007}/H_{\beta} = 1.1$) are typical of LINER galaxies (Veilleux & Osterbrock 1987). A spectrum extracted 4" (1.1 kpc) south of the nucleus (Fig. 4c) features absorption lines only; it is dominated by stars older than 10 Gyr. A spectrum extracted 8" (2.2 kpc) north of the nucleus (Fig. 4e) shows emission lines typical of HII regions and hence discloses here a star forming region.

The velocity field of NGC 5291 has been determined from the 2D spectral information along the S–N direction, given by the slit spectroscopy. We used the FCQ method developed by Bender (1990), with, as template, a spectrum of NGC 4478. The projected velocity profiles of the emitting gas and the stars are shown in the inset in Fig. 5. The gas and stellar velocities are in good agreement in the central regions but seem to diverge in the northern region. Stars appear to counter-rotate along the major-axis with respect to the ionized gas, and at a larger scale with the HI gas. We do not have any information about the kinematics along the minor axis.

The presence in NGC 5291 of morphological distortions, dust lanes, star forming regions and a counter-rotation strongly suggests that this early type galaxy has accreted in the past ex-

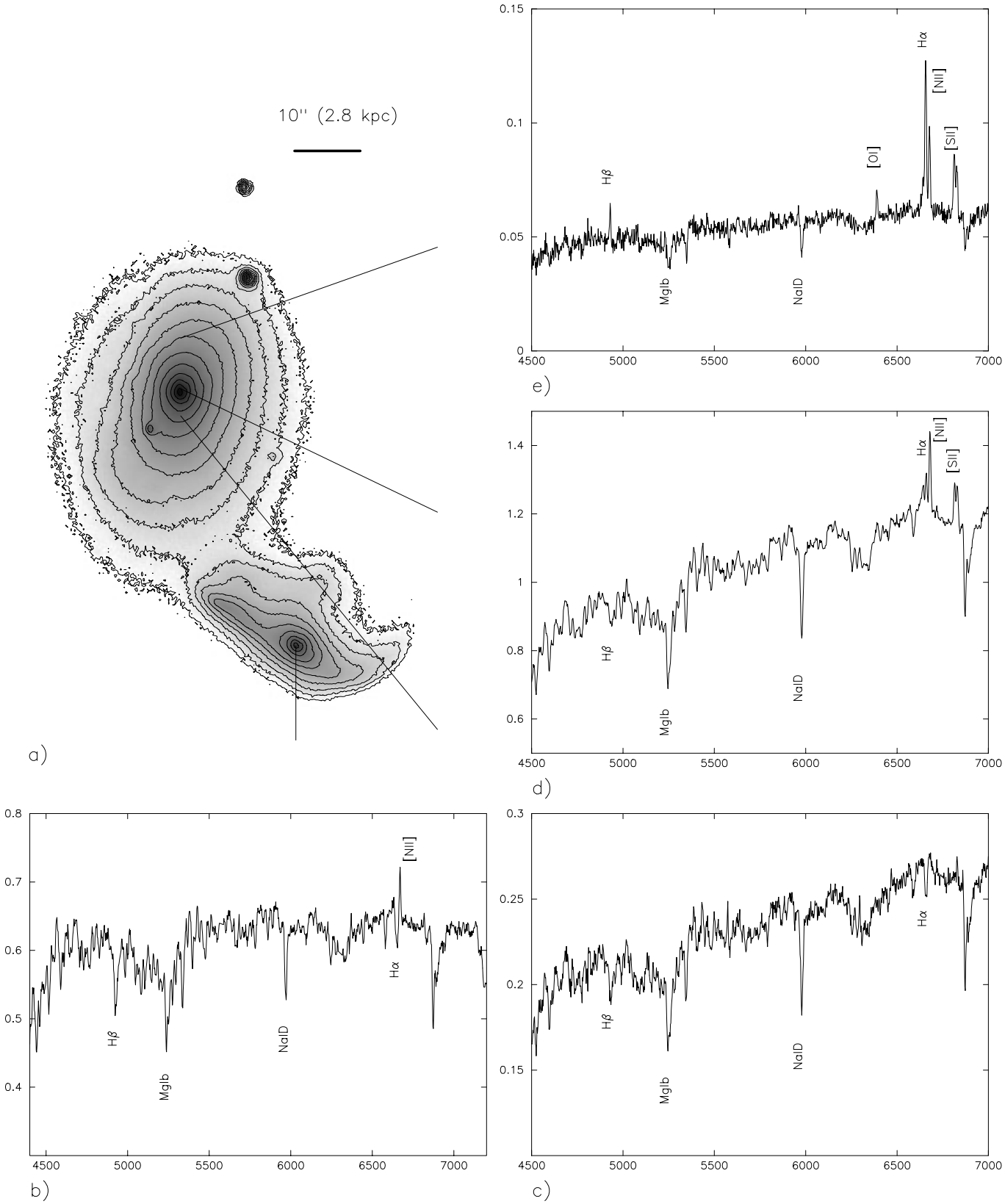


**Fig. 4. a** R band contour map of NGC 5291/Seashell. Levels are separated by 0.5 mag/$\square''$. **b–e** Optical spectra of the nuclei of the Seashell (**b**) and NGC 5291 (**d**), of a region situated 4" to the South (**c**), and of an HII region situated 8" to the North (**e**). Flux units are $10^{-15}$ erg cm$^{-2}$ s$^{-1}$ Å$^{-1}$.

**Table 5.** Spectrophotometry of the brightest knots

| Line | center | f | Observed, corrected fluxes relative to $H_\beta$ =100 | | | | |
|---|---|---|---|---|---|---|---|
| | | | Knot a | Knot g | Knot h | Knot i | Knot j |
| H$\delta$ | 4101.7 | 0.202 | 26±3, 30 | + [a] | + | + | + |
| H$\gamma$ | 4340.5 | 0.135 | 37±3, 41 | 32±6, 38 | - [b] | 44±1, 44 | 42±6, 44 |
| [OIII] | 4363.2 | 0.132 | - | - | - | 3±1, 3 | - |
| HeI | 4471.7 | 0.105 | 6±2, 7 | - | - | 4 ±1, 4 | - |
| H$\beta$ | 4861.3 | 0.000 | 100±3 | 100±7 | 100±9 | 100±1 | 100±6 |
| [OIII] | 4958.9 | -0.02 | 66±2, 65 | 65±8, 63 | 71±9, 71 | 86±1, 85 | 55±8, 55 |
| [OIII] | 5006.9 | -0.028 | 201±3, 197 | 194±7, 187 | 188±9, 186 | 257±2, 256 | 189±8, 187 |
| HeI | 5875.6 | -0.21 | 10±2, 8 | - | 13:±8, 12: | 11±0.5 | - |
| [OI] | 6300.3 | -0.285 | 6±3, 5 | 21±8, 14 | - | 6±1, 6 | - |
| [OI] | 6363.8 | -0.301 | 5±2, 4 | 7:±6, 5: | - | 2 ±1, 2 | - |
| [NII] | 6548.1 | -0.332 | 30±1, 23 | 31±4, 21 | 33±4, 28 | 18±0.5, 17 | 24±3, 21 |
| H$\alpha$ | 6562.8 | -0.335 | 362±2, 285 | 431±7, 285 | 332±6, 285 | 300±1, 285 | 319±4, 285 |
| [NII] | 6583.4 | -0.340 | 81±2, 64 | 105±4, 69 | 93±5, 80 | 63 ±0.5, 60 | 67±3, 60 |
| HeI | 6678.2 | -0.36 | - | - | - | 3±0.5, 3 | - |
| [SII] | 6716.4 | -0.369 | 49±2, 37 | 67±4, 43 | 55±6, 47 | 33±0.5, 31 | 47±7, 41 |
| [SII] | 6730.8 | -0.371 | 29±1, 22 | 45±4, 29 | 42±5, 36 | 25±0.5, 24 | 26±5, 23 |
| HeI | 7065.3 | -0.4 | - | - | - | 2±0.5, 2 | - |
| [ArIII] | 7135.8 | -0.412 | - | - | - | 9±0.5, 8 | - |
| [OII] | 7320, 30 | -0.435 | - | - | - | 6 ±0.5 | - |
| c | | | 0.31 | 0.54 | 0.20 | 0.07 | 0.14 |
| flux ($H_\beta$) ($10^{-15}$ erg cm$^{-2}$ s$^{-1}$) | | | 3.83 | 1.42 | 0.89 | 7.72 | 0.89 |
| eqw ($H_\beta$) (Å) | | | 145 | 82 | 112 | 140 | 69 |

[a] not observed;[b] not detected

**Table 6.** Spectrophotometry of the other knots

| Line | center | f | Observed and corrected fluxes relative to $H_\beta$ =100 | | | | | |
|---|---|---|---|---|---|---|---|---|
| | | | Knot b | Knot c | Knot d | Knot e | Knot f | Knot k |
| H$\gamma$ | 4340.5 | 0.135 | + | 42±12, 42 | 75±18, 75 | 61±21, 61 | + | + |
| H$\beta$ | 4861.3 | 0.000 | 100±10 | 100±8 | 100±22 | 100±14 | 100±22 | 100±15 |
| [OIII] | 4958.9 | -0.02 | 90±12, 89 | 53±12, 53 | 59±21, 59 | 48±15, 48 | 26±47, 26 | 73±12, 73 |
| [OIII] | 5006.9 | -0.028 | 236±10, 233 | 123±9, 123 | 240:±19, 240: | 126±15, 126 | 117:±16, 117: | 197±12, 197 |
| [NII] | 6548.1 | -0.332 | 25:±16, 21: | 11:±6, 11: | 23±11, 23 | 29±5, 28 | 25±7, 25 | 23±6, 22 |
| H$\alpha$ | 6562.8 | -0.335 | 339±11, 285 | 257±7, 257 | 277±13, 277 | 290±9, 290 | 288±10, 285 | 301±12, 285 |
| [NII] | 6583.4 | -0.340 | 44±5, 37 | 65±6, 65 | 69±10, 69 | 58±8, 57 | 79±9, 78 | 65±8, 62 |
| [SII] | 6716.4 | -0.369 | 25±6, 21 | 34±9, 34 | 35±10, 35 | 89±9, 88 | 46±9, 45 | 49±6, 46 |
| [SII] | 6730.8 | -0.371 | 22±6, 18 | 13±6 | 27 ±10, 27 | 46±7, 45 | 32±8, 31 | 40±6, 37 |
| c | | | 0.22 | 0.00: | 0.00: | 0.02 | 0.01 | 0.07 |
| flux ($H_\beta$) ($10^{-15}$ erg cm$^{-2}$ s$^{-1}$) | | | 0.47 | 0.22 | 0.16 | 0.20 | 0.21 | 0.41 |
| eqw ($H_\beta$) (Å) | | | 22 | 80 | 70 | 34 | 61 | 72 |

ternal material from cluster galaxies. L79 and later on MSGH97 have shown the puzzling spatial association of NGC 5291 with high quantities of HI mass. We confirm that the systemic optical velocity of the galaxy matches well that determined from the 21 cm line (see Fig. 5). We will discuss in Sect. 4.2 the hypothesis that the atomic gas was collected by NGC 5291 from other cluster galaxies.

### *3.2. The Seashell*

The optical and NIR images (Fig. 1 and Fig. 2) of the Seashell reveal a perturbed morphology. Its caustic structure is characteristic of a tidally disrupted disk at the early phases of an interaction (see for example the numerical simulations by Wallin 1990). The V-K' color map (Fig. 1b) suggests the presence of dust along a disk-like structure.

The nuclear spectrum (Fig. 4b) shows strong absorption Balmer lines. Only $[NII]_{\lambda 6584}$ is seen in emission. It is obvi-

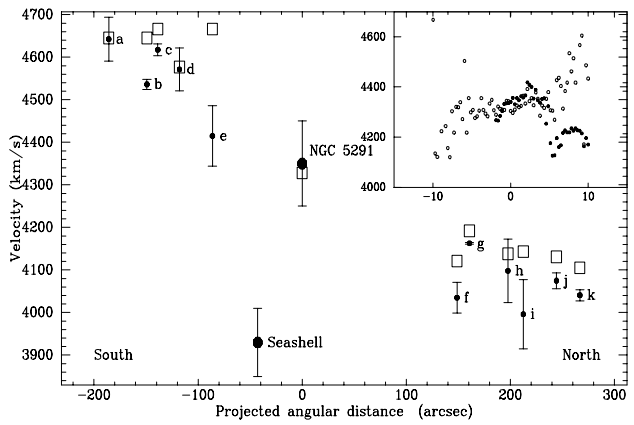


**Fig. 5.** Velocity profile of NGC 5291 along the S–N direction. The x-axis is the projected angular distance to the nucleus of NGC 5291. The full dots indicate the optical velocities of the knots and the squares the velocity of the associated HI clouds. The velocities of the parent galaxies are also indicated. The error bars take into account velocity gradients. The inset shows the internal kinematics of NGC 5291 along the S–N axis. The stars (empty dots) are counter-rotating with respect to the ionized gas (full dots).

ously more typical of an early type galaxy than of a spiral galaxy with a collision induced starburst. Based on NIR spectroscopic data, MSGH97 claim that it can not even be a post-starburst object. At the mean optical velocity of the Seashell (Table 2), MSGH97 did not detect any HI, suggesting that the galaxy was initially gas-poor.

The relative velocity of the Seashell is higher than 400 km $s^{-1}$ with respect to the velocity of NGC 5291. This galaxy appears therefore to be rather a fly-by than a strongly interacting partner [2].

### *3.3. The optical knots associated with the HI ring*

Fig. 1 discloses the presence of diffuse knots all along the eastern part of the HI ring. Our field does not reach its western part, but an image from the Digitalized Sky Survey (superimposed in Fig. 1) shows clearly elongated structures corresponding to the positions of the HI western condensations. Table 7 presents the integrated photometric properties of the optical knots and their HI gas content taken from MSGH97. Note however that the one to one match between the optical and HI features is not always possible since the visible and radio observations have different angular resolutions. The two brightest objects (Knot a and Knot i, or F and B in the nomenclature by L79), have blue absolute magnitudes of -15.5 and -16.4 resp. (see Table 7, Col. 2) and central blue surface brightness of 22.3 and 21.5 mag/$\Box''$ resp., values typical of blue compact galaxies. They are associated with two of the most prominent HI clumps. Their HI masses are greater than $10^9$ $M_\odot$. The other optical knots embedded in less massive clouds have absolute magnitudes also in the range of dwarf galaxies, but have a lower surface brightness: $23 - 23.5$ mag/$\Box''$. All these entities are extremely blue, with an average B-V=0.3 (Table 7, Col. 3), which implies that they are facing strong starbursts. Knot a and Knot i were detected in the near-infrared. Their positions are indicated by an arrow in Fig. 2. Their V-K' color of 2.0 (Table 7, Col. 4) is also rather blue but somehow higher than for BCDGs.

All 12 objects that we studied in the HI ring, but one, exhibit strong emission lines. The spectra are typical of HII regions ionized by massive young stars (see Fig. 3a–db-d). They show very weak continuum emission. The equivalent width of $H_\beta$ reaches 150 Å, a value characteristic of a very young starburst. The physical properties of the ionized gas, including its extinction and metallicity, will be discussed in Sect. 4.1. These star-forming objects are gas-rich, with $M_{\rm HI}/L_{\rm B}$ as high as 10 $M_\odot/L_\odot$ (Table 7, Col. 6). The peak column density of all HI clouds that collapsed to form stars is above $3\times10^{20}$ $cm^{-2}$ (MSGH97). Kennicutt (1989) discussed a critical threshold in the HI column density for the occurrence of star formation in spiral galaxies; Taylor et al. (1994) found it to be similar in HII galaxies. A threshold seems to apply also for the star-forming dwarfs around NGC 5291. It is striking however that we did not find any object brighter than $\mu_{\rm B} = 24$ mag/$\Box''$ at the position of the most massive HI clump, 1.5' north of the elliptical, although its peak column density there is greater than $10^{21}$ $cm^{-2}$. Since this HI clump is the closest to the parent galaxy, one may argue environmental effects to explain the inhibition of the star formation there.

The heliocentric velocities of the optical knots derived from the redshifts of the brightest lines are listed in Col. 5 of Table 3. The errors come from the standard deviation of the individual line measures. The velocities of the brightest knots compare well with those determined by L79, indicated in Col. 6. The HI velocities, measured at the location of the optical knots, are listed in Col. 7. Fig. 5 presents the optical (black dots) and HI velocity (empty squares) profiles along the HI eastern structure. Both are similar, confirming the physical association of the optical knots with the HI ring. The small discrepancies between the HI and the optical may be observational and due to the difference in the spatial resolutions in the two spectral domains. In particular, we will show in Sect. 4.1 that the ionized gas in some knots exhibits velocity gradients that would not have been observed in the radio.

### *3.4. Other objects*

We picked up three other galaxies in our MOS frames, indicated in Fig. 3a–d. Object "C" is an elliptical belonging to the cluster. Its optical velocity is 4700 km $s^{-1}$. Its spectrum shows Balmer absorption lines. Objects "1" and "2" are background starburst-like galaxies with redshifts of 0.074 and 0.202 resp.

[2] There is a discrepancy between our velocity measurement and that of L79, 200 km $s^{-1}$ lower. According to L79, the relative velocity of the Seashell would be 600 km $s^{-1}$. Our redshift was determined from a cross-correlation with a template galaxy with well determined redshift.

**Table 7.** Integrated properties of the tidal dwarfs

| Object | $M_B$ [a] | B-V [a] | V-K' [a] | $M_{HI}$ [b] | $M_{HI}/L_B$ |
|---|---|---|---|---|---|
| | mag | mag | mag | $10^9$ $M_\odot$ | $M_\odot/M_\odot$ |
| (1) | (2) | (3) | (4) | (5) | (6) |
| Knot a | -15.54 | 0.22±0.02 | 2.00±0.10 | 0.91 | 3.6 |
| Knot b | -14.13 | 0.22±0.03 | | 0.13 | |
| Knot c | -12.13 | 0.19±0.10 | | | |
| Knot d | -13.83 | 0.44±0.06 | | 0.54 | 10.1 |
| Knot e | -14.57 | 0.47±0.03 | | 0.43 | 4.1 |
| Knot f | -13.83 | 0.44±0.01 | | | |
| Knot g | -14.16 | 0.41±0.04 | | | |
| Knot h | -13.98 | 0.22±0.04 | | | |
| Knot i | -16.38 | 0.31±0.01 | 1.99±0.05 | 2.48 | 4.4 |
| Knot j | -13.74 | 0.21±0.04 | | | |
| Knot k | -13.40 | 0.35±0.05 | | | |

[a]: corrected for galactic extinction
[b]: from Malphrus et al. (1997)

## 4. Discussion

The following discussion mainly focuses on the properties of the optical counterparts of the HI clumps in NGC 5291. We will show that they were most probably formed after a tidal disruption of the HI disk associated with NGC 5291, and are therefore "tidal dwarf galaxies" (TDGs).

### *4.1. Properties of the optical knots*

The physics of 11 optical knots associated with the HI ring is studied here in details. Table 9 displays some integrated properties derived from our spectrophotometric data: the $H_\beta$ luminosity corrected for total extinction, the absorption in the blue, the Star Formation Rate and an estimate of the metallicity. The first 5 objects listed are those with the smallest uncertainties (see Sect. 2.2).

#### 4.1.1. Metallicity

A direct determination of the heavy element abundances, in particular the oxygen abundance, in the ionized gas requires the knowledge of the electron temperature and density of the O++ region. The flux ratio $([OIII]_{\lambda4959} + [OIII]_{\lambda5007})/[OIII]_{\lambda4363}$, particularly sensitive to the electron temperature $T_e$(OIII) , may be used to determine it. Unfortunately the $[OIII]_{\lambda4363}$ line is weak, especially in metal rich regions. $[OIII]_{\lambda4363}$ is barely seen in Knot i only (see Fig. 3a–dc). This $3\sigma$ detection should be considered as an upper limit. L79 and Peña et al. (1991) also claim a weak detection for that line. Our limit $[OIII]_{\lambda4363}/H_\beta = 0.03$ is consistent with the upper limit of 0.046 given by Peña et al. (1991). We have used the "nebular" package within IRAF to determine the physical parameters of Knot i and its ionic abundances. We measured an upper limit for $T_e$(OIII) of 12700 K. From the electron density diagnostic $[SII]_{\lambda6717}/[SII]_{\lambda6731}$, we found $Ne = 120$ cm$^{-3}$. Because of the limited number of diagnostic lines available with a high enough S/N, we have first assumed that the electron density and temperature were constant in the whole HII region and were in particular the same in the O+ and O++ regions. Our spectral coverage did not reach the $[OII]_{\lambda3727}$ line. Taking for the $[OII]_{\lambda3727}$ line flux the value measured by Pena et al. (1991) – $[OII]_{\lambda3727}/H_\beta = 3.71$ –, we have determined the following lower values for the ionic abundances:

$$12 + \log(\frac{O+}{H}) = 7.75 \pm 0.1$$

$$12 + \log(\frac{O++}{H}) = 7.65 \pm 0.06$$

This gives, with the previous approximation, a total oxygen abundance $12 + \log(\frac{O}{H})$ of:

$$12 + \log(\frac{O}{H}) = 12 + \log(\frac{O+ + O++}{H}) = 8.0 \pm 0.1$$

We have actually also detected weak [OII] lines at 7320/30 Å. With the temperature diagnostic $[OII]_{\lambda3727}/ [OII]_{\lambda7320,30}$, we have obtained $T_e$(OIII)=9200 K, a ionic abundance for O+ of 8.3, and a total oxygen abundance of 8.4. Therefore it most likely that the O abundance in the HII region of Knot i is largely greater than 8.

In the absence of the $[OIII]_{\lambda4363}$ line, the oxygen abundance of the other knots can be estimated with empirical diagrams introduced by Edmunds & Pagel (1984). Their method based on the measure of the single excitation parameter, $[OIII]/H_\beta$, suffers from larger uncertainties – typically 0.2 dex – and an ambiguity. For a given excitation, the O abundance can be read on two curves. We have parameterized the curves of Edmunds & Pagel (1984) (their Fig. A1) by the following equations:

$$12 + \log(\frac{O}{H}) = -0.68 \log(\frac{I([OIII]_{\lambda4959}) + I([OIII]_{\lambda5007})}{I(H_\beta)}) + 8.74$$

for the upper branch and

$$12 + \log(\frac{O}{H}) = 1.74 \log(\frac{I([OIII]_{\lambda4959}) + I([OIII]_{\lambda5007})}{I(H_\beta)}) + 6.35$$

for the lower branch.

The metallicity of Knot i obtained from the lower branch, 7.3, is inconsistent with the lower limit of 8.0 derived using $T_e$(OIII). Therefore the oxygen abundances should preferentially be read from the upper branch. The abundances estimated with that hypothesis are presented in Table 9 (Col. 5). The values determined with different methods for Knot i are summarized in Table 8. This table gives in particular estimates based on the more reliable parameter $R23 = ([OIII]_{\lambda4959} + [OIII]_{\lambda5007} + [OII]_{\lambda3727})/H_\beta$ (Skillman 1989b; Torres-Peimbert et al. 1989). The mean oxygen abundance of all the knots is 8.5 or $Z/Z_\odot = 0.36$, with a rather small dispersion. This value is much higher than that derived in typical blue compact galaxies (commonly $Z < Z_\odot/10$).

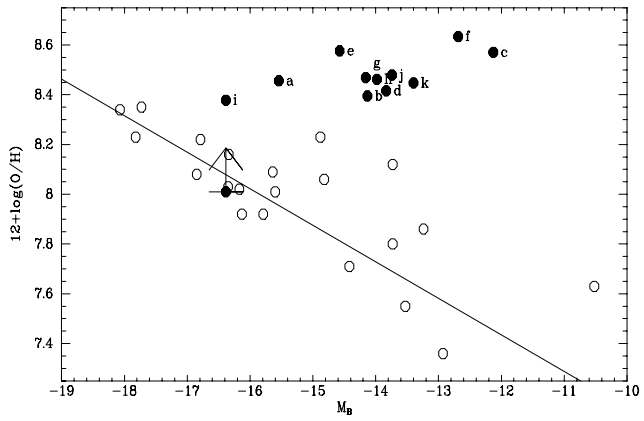


**Fig. 6.** Metallicity vs absolute blue magnitude for the tidal dwarfs in NGC 5291 (black points) and a sample of isolated dwarf irregular galaxies (open points; from Richer & McCall 1995). The oxygen abundances have been estimated with the empirical method of Edmunds & Pagel (1984), using the upper branch of their Table A1. A lower limit for the metallicity of Knot i, derived using its electron temperature, is indicated by an arrow. The tidal dwarfs deviate from the universal correlation between luminosity/mass and metallicity.

Fig. 6 shows the O abundance vs the absolute blue magnitude for all optical knots. A correlation has been well established between luminosity (hence mass) and metallicity for classical dwarf and giant galaxies (e.g. Skillman et al. 1989; Richer & McCall 1995; Skillman et al. 1997). A sample of nearby dwarf irregular galaxies with well determined metallicities, from the list of Richer & McCall (1995), has been added in Fig. 6. It is clear that the dwarf galaxies in the HI ring of NGC 5291 do not follow the luminosity–metallicity relationship. They roughly keep the same metallicity over a range of 4 magnitudes and seem to be too metal–rich for their luminosity. Such a discrepancy can be understood if the dwarf galaxies have not been much polluted by metal production during the recent star-formation episodes. The uniformity of their metallicity would be a consequence of a uniform pre-enrichment of the HI clouds in which they were formed. In this respect the dwarfs in NGC 5291 differ from classical BCDGs that were likely formed in primordial gas clouds.

A relative high metallicity for galaxies born out of tidally expelled material had already been noticed in studies of the interacting systems NGC 4038/39 (Mirabel et al. 1992), Arp 105 (Duc & Mirabel 1994), NGC 7252 (Duc 1995) and NGC 2992 (Duc et al. 1998, in preparation).

We have estimated an O abundance of $8.7 \pm 0.2$ for the HII region in NGC 5291 (see Table 2) from [OIII] and $H_\beta$ fluxes corrected for stellar absorption and the empirical method of Edmunds & Pagel (1984). This value is slightly higher than the metallicity of the optical knots. The excess could be due to a local enrichment by the galaxy itself.

**Table 8.** Oxygen abundance of Knot i

| | |
|---|---|
| Empiral method: | |
| + From the excitation parameter: | |
| 12+log(O/H) upper | $8.38 \pm 0.2$ |
| 12+log(O/H) lower | $7.28 \pm 0.2$ |
| + From R23: | |
| R23 | $0.85 \pm 0.07$ |
| 12+log(O/H) upper | $8.38 \pm 0.2$ |
| 12+log(O/H) lower | $7.67 \pm 0.2$ |
| Physical method: | |
| $T_e$(OIII) | $< 12700$ K $\pm 600$ K |
| $Ne$ | 120 cm$^{-3}$ |
| 12+log(O+/H+) | $> 7.75 \pm 0.1$ |
| 12+log(O++/H++) | $> 7.65 \pm 0.06$ |
| 12+log(O/H) | $> 8.00 \pm 0.1$ |

**Table 9.** Properties of the TDG HII regions

| Object | $L$H$_\beta$ $10^{38}$ erg s$^{-1}$ | $A_B$ mag | SFR M$_\odot$ yr$^{-1}$ | 12+log(O/H) upper |
|---|---|---|---|---|
| (1) | (2) | (3) | (4) | (5) |
| Knot a | 15.5 | 0.88 | 0.031 | 8.46 |
| Knot g | 5.7 | 1.53 | 0.012 | 8.47 |
| Knot h | 3.6 | 0.56 | 0.005 | 8.46 |
| Knot i | 31.2 | 0.19 | 0.063 | 8.38 |
| Knot j | 3.6 | 0.41 | 0.007 | 8.48 |
| Knot b | 1.9 | 0.63 | 0.004 | 8.39 |
| Knot c | 0.9 | 0.00: | 0.002 | 8.57 |
| Knot d | 0.6 | 0.00: | 0.001 | 8.41 |
| Knot e | 0.8 | 0.06: | 0.002 | 8.57 |
| Knot f | 0.8 | 0.04: | 0.002 | 8.63 |
| Knot k | 1.7 | 0.20 | 0.002 | 8.45 |

#### 4.1.2. Extinction

The absorption in the blue, derived from the Balmer decrement, seems to differ significantly from one object to the other (see Table 9, Col. 3). For instance, the total absorption of the two brightest knots a and i differs by 0.7 mag. Taking into account the galactic absorption in the direction of NGC 5291, our measurements indicate that Knot i suffers very little redenning whereas the extinction in Knot a is at least 0.5 mag. This result is surprising given the rather uniformity of the metallicities noticed here above, and favors local effects. No correlation is found between $A_B$ and the H$_\alpha$ flux.

#### 4.1.3. Current star formation

Almost all the dwarfs in the HI ring experience active star formation episodes. We estimated the current star formation rate from the H$_\alpha$ luminosity and the formula $SFR(\mathrm{M}_\odot\ \mathrm{yr}^{-1}) = 7.07\times10^{-42} L_{\mathrm{H}\alpha}(\mathrm{erg\ s}^{-1})$, valid for 0.1–100 M$_\odot$ (Hunter &

Gallagher 1986). The $SFR$, given in Table 9 (Col. 4), ranges between 0.001 $M_\odot$ yr$^{-1}$ and 0.063 $M_\odot$ yr$^{-1}$.

The mean equivalent width of the $H_\beta$ line (see Table 5) is 80 Å, a value comparable to that of HII galaxies (Terlevich et al. 1991). The highest values measured on Knot a and Knot i, 140 Å, indicate that the current starburst in these objects is extremely young. Evolutionary synthesis models of instantaneous bursts by Cerviño & Mas-Hesse (1994) or Leitherer & Heckmann (1995) constrain the burst to be younger than 4 Myr, whatever the assumed metallicity. A Wolf-Rayet bump between rest-wavelengths 4630–4690 Å is barely detected in Knot i (see Fig. 3a–dc). Its equivalent width is 3 Å. Given that value, the model of Cerviño & Mas-Hesse (1994) for metallicities similar to those of the NGC 5291 dwarfs – $Z_\odot/3$ – further restricts an age between 3 Myr and 5 Myr.

#### 4.1.4. Stellar populations

The continuum of the optical knots is extremely low and does not exhibit any absorption features tracing evolved stars. Indirect indications for the absence/presence of an old stellar population may be obtained from optical and infrared photometry. During the first 5 Myr of the burst, most of the light is dominated by the contribution of the gas ionized by OB stars; the line emission dominates in the optical broad-band filters (60–80 % in R) whereas the continuum emission prevails in the near-infrared ($\sim$ 50 % in K) (Krüger et al. 1995). The NIR colors of Knot i corrected for galactic extinction – J-H=0.39; H-K'=0.73 – are those expected for pure gas continuum emission (J-H=0.29,H-K=0.72; Krüger et al. 1995). The contribution from hot dust is negligible. On the H-K' vs J-H color-color diagram, Knot i is situated well outside the tracks of red giant stars (Thuan 1985), which confirms the absence of evolved stars.

However a V-K' index of 2.0, corrected for galactic extinction, as measured for Knot a and Knot i appears to be rather red compared to the color of young blue compact galaxies (Thuan 1983; Thuan 1985), and that predicted by models of young starbursts. A V-K' of 0.5, independent of metallicity, is expected for bursts aged between 3 Myr and 5 Myr (Cerviño & Mas-Hesse 1994). During the red-supergiant phase, between 10-15 Myr, V-K=2 can be reached for a metallicity similar to that of NGC 5291 dwarfs, whereas during this phase a much bluer V-K color is predicted for metal deficient objects like BCDGs. A reddening is expected for bursts younger than 3 Myr, but its level is uncertain due to the errors of the models at the burst onset. Therefore the age constrained by V-K seems higher than what the NIR colors and spectrophotometric data predict. This could indicate problems with the models or the observations. It more probably means that the star formation extended during a period of about 10 Myr, with the current burst being younger than 5 Myr. Further investigations using the whole spectral energy distribution and updated evolutionary synthesis models are in preparation (Fritze-v.Alvensleben & Duc 1997).

In any cases, the available data show no evidence for the presence of an old stellar population contributing significantly to the overall stellar population of the knots in NGC 5291.

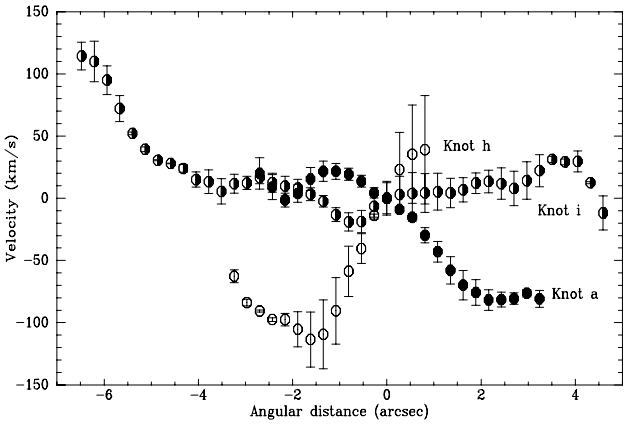


**Fig. 7.** Velocity profiles of the ionized gas of Knots a, i and h along the S–N direction.

#### 4.1.5. Dynamics

We witness in the HI ring of NGC 5291 the collapse of HI clumps leading to the formation of independent entities. Some kinematical signatures of such instability should be observable. It is also expected that after a while, these objects become gravitationally bound and start even rotating, as it was likely observed for the dwarf galaxy in the tidal tail of Arp 105 (Duc et al. 1997a). Unfortunately the spatial resolution of the HI observations is too low to directly investigate the velocity field of knots that have an angular size of 5–10". Instead MSGH97 used the velocity width of the HI lines to claim that Knot i (their Knot B) is gravitationally bound. Slit spectroscopy of the ionized gas provides with a better sampling limited by the seeing (1.5" for our observations) along one spatial dimension. Fig. 7 shows the velocity profiles along the S–N direction for three of the brightest knots. The velocities were determined from the redshifts of the brightest lines. The spatial axis originates at the peak of the $H_\alpha$ emission; the velocity is relative to that position. Gradients steeper than 100 km s$^{-1}$ over distances of 3 $''$ are seen, with indications of flattening at the edges. At the distance of NGC 5291, this translates into a gradient of at least 120 km s$^{-1}$/kpc. It would be premature to impute these motions to rotation because we do not know the 3D velocity field and orientation of the objects. If nevertheless we speculate that Knots a and i are seen face-on and that the S-N direction is their main rotation axis, we derive a dynamical mass of $2\times10^9$ $M_\odot$, inside their optical radius. This mass is of the same order as the masses of the associated HI clouds, meaning that the objects would still essentially be in a gaseous phase, and contain little stellar and dark matter. Note also that Knot i would counter-rotate with respect to the HI ring.

### *4.2. Origin of the HI in NGC 5291*

The physical association between the HI ring-like structure and the early-type galaxy NGC 5291 seems to be well established. In particular the systemic optical velocity of the galaxy corresponds exactly to the central velocity of the HI rotation curve (see Fig. 5). However the quantity of HI involved –

$4.9\times10^{10}$ $M_\odot$ (MSGH97) – is extremely important for a lenticular object. An HI mass to blue luminosity ratio of $2.4\,M_\odot/L_\odot$, as measured in NGC 5291, is not even observed in normal gas-rich spirals. An external origin for the HI observed in elliptical and lenticular galaxies is commonly proposed (e.g. Knapp et al. 1985; Bertola et al. 1992). The atomic gas in NGC 5291 cannot originate from a primordial intergalactic cloud. The mean metallicity we estimated in its underlying HII regions, $Z_\odot/3$, is too high; later large-scale enrichment by the the parent galaxy itself is unlikely since the HI is much more extended than the galaxy. More probably the lenticular has accreted this gas from a companion during interaction/merger events. Indeed we have noticed in the core of the galaxy several features which may be remnants of previous collisions: in particular the presence of a dust arc, a star-forming region, and a counter-rotation of the gas with respect to the stars.

The atomic gas could have been supplied by one of the cluster companions near NGC 5291. Direct mass transfers between a spiral and an elliptical have already been observed, for e.g. in the interacting system Arp 105 (Duc et al. 1997a). The nearby Seashell galaxy is an unlikely gas-provider candidate though, since this galaxy was probably originally gas-poor (see Sect. 3.2). Another hypothesis is that NGC 5291 absorbed in its past one or several gas-rich objects. One can exclude the involvement of dwarf galaxies. The number of merger events required would be too high to account for the high HI mass observed. NGC 5291, although it is not a very luminous galaxy, could be the result of a merger between two spirals and be therefore a post-starburst, in a far more advanced stage than the typical merger NGC 7252. No long stellar tails, remnants of a disk-disk collision, are indeed observed. A similar explanation was recently proposed by Morganti et al. (1997) for the origin of the HI in the elliptical galaxy NGC 5266. Such an event would have therefore occured long before the recent encounter between NGC 5291 and the Seashell.

The structure of the HI distribution itself – an asymmetric ring – is puzzling. L79, Duc (1995) and recently MSGH97 extensively discussed its origin.

Appleton (1983) suggested that the infall of gas from a tidally disrupted galaxy could directly lead to the formation of a ring. However, apart from the gas-poor Seashell, there is no obvious remnant of such a disrupted object in the vicinity of NGC 5291. On the other hand, there is a strong resemblance between the ring in NGC 5291, the huge HI ring discovered by Schneider (1989) around M105 in the M96 group, and, at a smaller scale, more classical ring galaxies. Numerical simulations have shown that high-speed head-on collisions form ring like structures in both the stellar and gaseous components. In NGC 5291, a large HI disk hit at high velocity by a companion galaxy – not necessarily the Seashell which appears to be too close to the target – could have produced the ring.

There is little doubt that the optical objects lying along the HI ring were formed simultaneously after the collapse of a single gas structure. There is an excellent match in position and velocity between the optical knots and the gas clumps. The uniformity of their metallicity distribution argue against the idea that they are pre-existing dwarf galaxies belonging to the cluster. The optical knots are therefore most likely second-generation, tidal, dwarf galaxies. What caused the fragmentation and collapse of the HI clouds to form TDGs is still not well understood, although in the case of NGC 5291, ram pressure effects by the intra-cluster medium could play a role. Hawarden & Chaytor (1996) discuss this hypothesis using X-ray observations of the system.

### *4.3. Tidal dwarf galaxies*

Optical and HI studies of a now significant number of interacting galaxies (Hibbard & van Gorkom 1996; Duc & Mirabel 1997) have shown that dwarf galaxies are often produced during galactic collisions. In all the systems studied so-far, only a few, generally one or two, TDGs were observed. In NGC 5291, more than 10 star-forming galaxies were produced. The vitality of such a galactic nursery could however only be apparent and the result of a time scale bias. The tidal dwarfs in NGC 5291 seem to be younger than in other interacting systems (Duc et al. 1997b). Hibbard & Mihos (1995), using numerical simulations, have predicted that a large part of tidally expelled material fall back on the parent galaxies within 1 Gyr after the collision. Dwarf galaxies in the vicinity of giant galaxies may also be tidally disrupted. Therefore it is expected that only the most massive and distant TDGs may survive. This means for NGC 5291 that probably only Knot a and Knot i, situated at resp.50 and 60 kpc from their parent, have a significant life expectancy and will become truly independent galaxies. Also the fact that the most massive HI clump, but also the closest to NGC 5291, has no optical counterpart, clearly shows that the formation of tidal dwarfs is not an easy process in the neighborhood of giant galaxies.

The discovery of velocity gradients in the ionized gas of the tidal dwarfs in NGC 5291 and Arp 105 (Duc et al. 1997a) supports the idea that some TDGs may be gravitationally bound. From the analysis of HI data, Duc et al. (1997a), Hibbard et al. (1997) and MSGH97 reached the same conclusion. Mainly because of a lack of angular resolution, it is not yet known whether TDGs are supported by rotation. Their dark matter content, which according to numerical simulations of interacting systems, should be low (Barnes & Hernquist 1992), is observationally not well constrained (see Sect. 4.1.5). Tridimensional optical spectroscopy of TDGs would be very helpful to address these issues.

The contribution of tidal dwarfs to the overall population of dwarf galaxies is largely unknown. In groups and clusters, it could be significant, as claimed by Hunsberger et al. (1996). Vilchez (1995) found that dwarf galaxies with companions also seem to deviate from the mass-metallicity relation and part of them may be recycled objects (Compare his Fig. 9 with our Fig. 6). Metallicity measurements appear indeed as a useful tool to identify a tidal origin in a dwarf galaxy once the stellar/gaseous tidal bridge that links it to its parent has dissipated. Incidently the fact that Knot i in NGC 5291 appeared in an Objective Prism Survey and was classified as an HII galaxy (Maza et al. 1991) is perhaps not so anecdotal. Some contamination in

catalogs of BCDGs by tidal dwarfs cannot be excluded, especially in clusters.

We finally note that young tidal objects like those in NGC 5291 are good laboratories to study the star formation in the local Universe. They are simple objects, still in a very early stage of their evolution and are not polluted by an old stellar component.

## 5. Conclusion

We have studied 11 extragalactic HII regions in the neighborhood of NGC 5291 and have clearly shown that they were born within the same HI ring-like structure associated with the galaxy. This perturbed lenticular has probably suffered one or several interactions in its past and accreted its hydrogen gas from other cluster galaxies. NGC 5291 could even be the result of an evolved complete merger between gas-rich spirals.

The brightest knots in the HI ring exhibit properties similar to those of blue compact galaxies: high central surface brightness; extremely blue colors; active star formation episodes. Their current burst is younger than 5 Myr. There is no compelling evidence for the presence of an old underlying stellar population; the galaxies may therefore be extremely young objects forming their first generation of stars. The main difference however between the dwarfs in NGC 5291 and classical dwarf galaxies is their high metallicity ($Z_{\odot}/3$) and the fact that they do not follow the mass-metallicity correlation. Contrary to the extremely metal poor BCDGs, they were not formed in primordial gas clouds but in HI clouds that were already pre-enriched in the outer parts of the pre-encounter parent galaxies. In this respect, the dwarfs in NGC 5291 are recycled galaxies and most probably belong to the recently studied class of "tidal dwarf galaxies".

*Acknowledgements.* We first wish to thank E. Simpson and S. Gottesman for providing us the HI-datacube long before the publication of the data. We are grateful to all the people at la Silla who helped us during the observations, especially the NTT team for the preparation of the MOS files, and C. Lidman for his precious recipes for reducing NIR data. Special thanks to E. Emsellem for his contribution in the dynamical study of the system, and U. Fritze-v.Alvensleben for fruitful discussions on photometric models. Finally, we thank our referee, E. Skillman, for his careful reading of the manuscript and useful suggestions. This study has made used of the NASA/IPAC Extragalactic Database (NED). The overlapped Digitalized Sky Survey in Fig. 1 is based on a photographic plate obtained using the UK Schmidt Telescope.

## References

Appleton, P. N.: 1983, MNRAS 203, 533
Barnes, J. E. & Hernquist, L.: 1992, Nature 360, 715
Bender, R.: 1990, A&A 229, 441
Bertola, F., Buson, L. M., & Zeilinger, W. W.: 1992, ApJ 401, L79
Casali, M. & Hawarden, T.: 1992, JCMT-UKIRT Newsletter 3, 33
Cerviño, M. & Mas-Hesse, J. M.: 1994, A&A 284, 749
Daly, P. N., Phillipps, S., & Disney, M. J.: 1987, A&AS 68, 33
Doublier, V. & Caulet, A.: 1996, BAAS 188, 0904
Duc, P.-A.: 1995, Ph.D. thesis, Université Paris VI
Duc, P.-A., Brinks, E., Wink, J. E., & Mirabel, I. F.: 1997a, A&A, 326, 537
Duc, P.-A., Fritze-v. Alvensleben, U., & Mirabel, I. F.: 1997b, in G. Mamon, T. Thuan, & T. Tran (eds.), Extragalactic Astronomy in the Infrared, Ed. frontieres
Duc, P.-A. & Mirabel, I. F.: 1994, A&A 289, 83
Duc, P.-A. & Mirabel, I. F.: 1997, Messenger 89, 14
Edmunds, M. G. & Pagel, B. E. J.: 1984, MNRAS 211, 50
Fritze-v.Alvensleben, U. & Duc, P.-A.: 1997, in Kyoto IAU 23, pp JD2–050P
Hamuy, M., Walker, A. R., Suntzeff, N. B., Gigoux, P., Heathcote, S. R., & Phillips, M. M.: 1992, PASP 104, 533
Hawarden, T. G. & Chaytor, D. H.: 1996, BAAS 189, 120.17
Hibbard, J., van der Hulst, J., & Barnes, J.: 1997, in preparation
Hibbard, J. E., Guhathakurta, P., van Gorkom, J. H., & Schweizer, F.: 1994, AJ 107, 67
Hibbard, J. E. & Mihos, J. C.: 1995, AJ 110, 140
Hibbard, J. E. & van Gorkom, J. H.: 1996, AJ 111, 655
Hunsberger, S. D., Charlton, J. C., & Zaritsky, D.: 1996, ApJ 462, 50
Hunter, D. A. & Gallagher, J. S.: 1986, PASP 98, 5
Kennicutt, R. C., J.: 1989, ApJ 344, 685
Knapp, G. R., Turner, E. L., & Cunniffe, P. E.: 1985, AJ 90, 454
Krüger, H., Fritze-V. Alvensleben, U., & Loose, H. H.: 1995, A&A 303, 41
Landolt, A. U.: 1992, AJ 104, 340
Leitherer, C. & Heckman, T. M.: 1995, ApJS 96, 9
Longmore, A. J., Hawarden, T. G., Cannon, R. D., Allen, D. A., Mebold, U., Goss, W. M., & Reif, K.: 1979, MNRAS 188, 285
Malphrus, B., Simpson, C., Gottesman, S., & Hawarden, T. G.: 1997, AJ 114, 1427
Maza, J., Ruiz, M. T., Gonzalez, L. E., Wischnjewsky, M., & Pena, M.: 1991, A&AS 89, 389
Mirabel, I. F., Dottori, H., & Lutz, D.: 1992, A&A 256, L19
Morganti, R., Sadler, E. M., Oosterloo, T., Pizzella, A., & Bertola, F.: 1997, AJ 113, 937
Papaderos, P., Loose, H. H., Thuan, T. X., & Fricke, K. J.: 1996, A&AS 120, 207
Peña, M., Ruiz, M. T., & Maza, J.: 1991, A&A 251, 417
Richer, M. G. & McCall, M. L.: 1995, ApJ 445, 642
Sanders, D. B. & Mirabel, I. F.: 1996, ARA&A 34, 749
Schneider, S. E.: 1989, ApJ 343, 94
Schweizer, F.: 1978, in E. Berkhuijsen & R. Wielebinski (eds.), Structure and Properties of Nearby Galaxies, p. 279, Dordrecht, D. Reidel Publishing Co.
Skillman, E. D.: 1989, ApJ 347, 883
Skillman, E. D., Bomans, D. J., & Kobulnicky, H. A.: 1997, ApJ 474, 205
Skillman, E. D., Kennicutt, R. C., & Hodge, P. W.: 1989, ApJ 347, 875
Smith, E. P. & Hintzen, P.: 1991, AJ 101, 410
Taylor, C. L., Brinks, E., Pogge, R. W., & Skillman, E. D.: 1994, AJ 107, 971
Terlevich, R., Melnick, J., Masegosa, J., Moles, M., & Copetti, M. V. F.: 1991, A&AS 91, 285
Thuan, T. X.: 1983, ApJ 268, 667
Thuan, T. X.: 1985, ApJ 299, 881
Thuan, T. X., Izotov, Y. I., & Lipovetsky, V. A.: 1997, ApJ 477, 661
Torres-Peimbert, S., Peimbert, M., & Fierro, J.: 1989, ApJ 345, 186
Veilleux, S. & Osterbrock, D. E.: 1987, ApJS 63, 295
Vilchez, J. M.: 1995, AJ 110, 1090
Wallin, J. F.: 1990, AJ 100, 1477